Proc. Natl. Acad. Sci. USA
Vol. 88, pp. 5503–5507, July 1991
Biophysics

Observation of the light-triggered binding of pyrone to chymotrypsin by Laue x-ray crystallography

(polychromatic x-ray crystallography/flash photolysis/serine protease/enzyme active site)

BARRY L. STODDARD*†, PAULA KOENIGS‡, NED PORTER‡, KYRIACOS PETRATOS§, GREGORY A. PETSKO*¶, AND DAGMAR RINGE*¶

*Massachusetts Institute of Technology, Department of Chemistry, Cambridge, MA 02139; ‡Duke University, Department of Chemistry, Durham, NC 27706; and §Institute for Molecular Biology and Biophysics-FORTH, P.O. Box 1527, 711 10 Heraklion-Crete, Greece

Communicated by Daniel E. Koshland, Jr., February 19, 1991

ABSTRACT **Crystals of γ-chymotrypsin inhibited with the photodissociable group *trans-p*-diethylamino-*o*-hydroxy-α-methylcinnamate were irradiated with a 1-msec flash from a high-energy xenon flashlamp in the presence of the mechanism-based inhibitor 3-benzyl-6-chloro-2-pyrone. The ensuing reaction was monitored by collection of sequential, single-exposure Laue x-ray diffraction patterns. The experiment was also performed in solution to verify the regeneration of catalytic activity and the subsequent inhibition of the enzyme by pyrone after photolysis. The resulting crystallographic structures show the presence of covalently bound cinnamate prior to photolysis, the generation of "free" enzyme after irradiation of the crystal, and the slow formation of a pyrone-inhibited complex several hours after photolysis. The structure of the free enzyme shows a significant proportion of the active sites in the crystal to contain a naturally occurring, noncovalently bound tetrapeptide inhibitor [Dixon, M. M. & Matthews, B. W. (1989) *Biochemistry* 28, 7033–7038], even after cinnamate acylation and photolysis. Data collected simultaneously with irradiation show the crystal to be slightly disordered during photolysis, leading to streaked x-ray photos. The resulting maps are suggestive of a bicyclic coumarin species produced by photolysis and deacylation; however, the electron density is difficult to model unambiguously by one unique chemical state. Nevertheless, Laue crystallography is shown to be capable of visualizing time-dependent chemical changes in the active site of an enzyme.**

The time needed to collect a high-resolution crystallographic data set for a macromolecule ranges from hours to weeks. This fact imposes serious restrictions on the direct crystallographic observation of intermediate structures during enzymatic catalysis. Two technical advances now show promise for direct structural studies of catalytic intermediates: the synchrotron x-ray source and the ability to process polychromatic x-ray diffraction patterns from crystalline macromolecules. Synchrotron radiation is extremely intense, 10^{11}–10^{12} photons per sec per mm^2 with a spectrum spanning approximately 0.4–2.0 Å or 6–25 keV of pulsed, polarized x-rays (1, 2). Direct use of the "white" x-ray beam from a synchrotron reduces the exposure time needed to collect a data set to ≈100 msec or less for a single shot. This technique is gaining popularity as a method for the structural analysis of biological macromolecules due to the development of computational methods for processing polychromatic diffraction patterns (3–9) and to the successful interpretation of protein difference maps calculated from the resulting data (1, 10–16).

The publication costs of this article were defrayed in part by page charge payment. This article must therefore be hereby marked "*advertisement*" in accordance with 18 U.S.C. §1734 solely to indicate this fact.

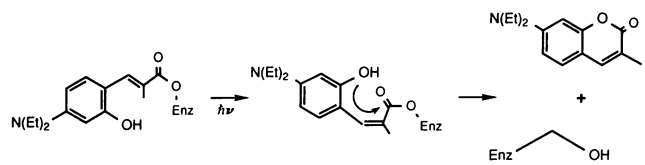

FIG. 1. Mechanism of photochemical deacylation of *trans-p*-diethylamino-*o*-hydroxy-α-methylcinnamate. Enz, enzyme.

To observe the structure of intermediate species during turnover, catalysis must be initiated simultaneously throughout the crystal so that the rate-limiting step is the decay of the intermediate structure of interest. For the work described here, enzymatic turnover was triggered through the photolysis of a photolabile inhibitor bound to the active-site serine of crystalline γ-chymotrypsin (Fig. 1). Covalently inhibited chymotrypsin was irradiated in the presence of the mechanism-based inhibitor 3-benzyl-6-chloro-2-pyrone (17). The ensuing reaction was monitored by collection of sequential Laue x-ray diffraction patterns.‖

MATERIALS AND METHODS

The crystallization of γ-chymotrypsin has been described (18, 19). Crystals were covalently inhibited in the dark by soaking against 240 mM *trans-p*-diethylamino-*o*-hydroxy-α-methylcinnamate (hereafter referred to as cinnamate). Twenty microliters of inhibitor stock (2.4 M, 600 mg/ml in dimethyl sulfoxide) was added to 180 μl of mother liquor [85% saturated $(NH_4)_2SO_4$ in 20 mM cacodylate, pH 7.4] containing a suitable crystal. The inhibitor is only sparingly soluble upon addition to the aqueous phase. The soak was continued for 6 weeks, with the mother liquor and inhibitor replaced every 7 days with a fresh suspension of inhibitor. Less thorough soaks cause incomplete acylation by the inhibitor and retention of a tetrapeptide that is found in the active site of native crystalline γ-chymotrypsin (14, 19, 20).

Photolysis and Data Collection. Studies were performed on Beamline X31 at the Deutsche Elektronen Synchrotron in Hamburg. Crystals of inhibited chymotrypsin were soaked in the dark for 3 days in cinnamate-free mother liquor at pH 7.4 containing 5% (vol/vol) acetonitrile and 5 mM 3-benzyl-6-chloro-2-pyrone (hereafter referred to as pyrone). Individual crystals were then mounted in 1-mm-diameter quartz capil-

Abbreviations: cinnamate, *trans-p*-diethylamino-*o*-hydroxyl-α-methylcinnamate; pyrone, 3-benzyl-6-chloro-2-pyrone.

†To whom reprint requests should be sent at present address: Department of Biochemistry, Barker Hall, University of California, Berkeley, CA 94720.
¶Present address: Rosenstiel Basic Medical Sciences Research Center, Brandeis University, Waltham, MA 02254.

‖The atomic coordinates and structure factors have been deposited in the Protein Data Bank, Chemistry Department, Brookhaven National Laboratory, Upton, NY 11973 (reference 4GCH, 5GCH).

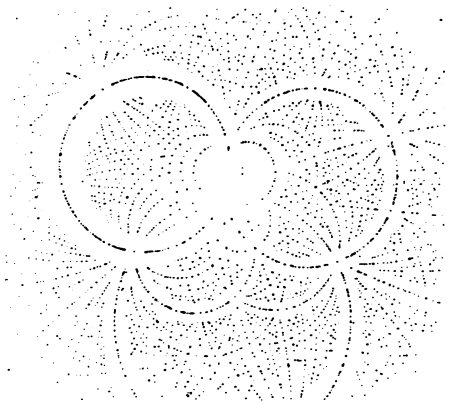

FIG. 2. Polychromatic x-ray Laue diffraction pattern.

laries filled with mother liquor plus 5 mM pyrone and sealed at both ends with wax. The crystals were held between plugs of cotton fibers. The crystal was cooled to 10°C and then flashed with a JML Xe flash system delivering up to 340 J per pulse over a broad spectrum from 300 to 700 nm (21). The flash duration was ≈1 msec. The lamp produces >1 kW in a cross-sectional area of ≈3 mm^2. The reaction then proceeded at room temperature.

Single-exposure diffraction patterns (Fig. 2) were collected using Kodak DEF x-ray film (6 films per pack) over a period ranging from $t = -5$ min (before irradiation), to $t = 0$ (simultaneous with photolysis) to $t = +24$ hr. Eight data sets were collected. Table 1 gives details of the data collection and processing.

Data Processing and Reduction. After autoindexing and positional refinement, the films were individually integrated using the program INTLAUE (9). Only reflections with $I > 2\sigma I$ were retained for further processing. The films within each pack were then scaled against one another and merged, after correction for the differential absorption of different wavelength reflections by the films. At this point an obliquity correction and the Lorentz-polarization correction were also applied. The data were then scaled to account for the varying spectrum intensity. The final data sets (Table 1) contained 3000–3400 unique reflections to 2.5-Å resolution, ≈25% of the total data between 5- and 2.5-Å resolution.

Structural Refinement and Map Calculations. Each data set was placed directly into least-squares refinement by using the structure of the "native" photolyzed chymotrypsin (19) as the initial model. No inhibitor coordinates or water molecules were included at any stage of these refinements. Sequential cycles of refinement were run until the protein geometry was satisfactory and the overall R factor had minimized. These refined R factors ranged from 17.2% to 22.9%.

Difference maps ($F_o - F_c$) were then calculated using the refined coordinates to supply phases and calculated structure factors. These maps were independently examined using the program FRODO (22) on an Evans and Sutherland (Salt Lake City) PS300 graphics display. For the maps in which unambiguous electron density for a bound species was present, the ligand was built into the structure and the refinement was continued. The ligands were completely unrestrained during these refinements. Table 1 shows the results of the final refinements.

The experiment was also performed in solution under similar conditions to confirm the observations in the crystallographic studies and to compare the solution-phase reactivity of photoactivated chymotrypsin with that of the crystalline form. A 1.4-ml aliquot of 43.6 μM (0.5 mg/ml) chymotrypsin (Sigma type I-S) in TBS (50 mM Tris·HCl, pH 7.4/150 mM NaCl) was inhibited with 133 μl of 2.7 mM cinnamate in methanol. When the inhibited enzyme was <5% active, the acylenzyme was purified using a Sephadex G-25 gel column with TBS. The fractions containing the acylenzyme were collected and diluted to 40 ml with TBS, producing a solution which upon photolysis yielded 1.4 mM active enzyme.

A 475-μl aliquot of cinnamoylchymotrypsin was mixed with 25 μl of 100 mM pyrone in acetonitrile, and the enzymatic activity was assayed. This solution and a control solution of inhibited chymotrypsin (no pyrone added) were photolyzed for 40 sec with a 500-W Hg lamp, and the change in enzymatic activity with time was monitored by chromogenic assay.

The assays were performed with 1 ml of 30 mM Tris·HCl, pH 8.3/3 mM $CaCl_2$/400 mM NaCl, 150 μl of 1 mM S-2586 (MeO-Suc-Arg-Pro-Tyr *p*-nitroanilide hydrochloride; Suc, succinyl), and 20 μl of photolyzed enzyme at room temperature. Assays were initiated by the addition of enzyme, and

Table 1. Data processing and structural refinement statistics for data sets* collected at −5 min to 24 hr

	−5 min	0 min	+1 min	+5 min	+10 min	+20 min	+3 hr	+24 hr
Exposure time, sec	5	5	5	5	5	5	10	10
Integration and interpack scaling								
A-film spots	5910	6226	5978	6002	6004	5989	5927	6059
A-film overall rms (pixels)	1.7	2.5	1.9	1.8	1.9	1.6	1.6	1.4
Film-to-film R factor, %	5.1	8.3	5.4	4.8	4.5	4.7	3.4	4.2
Reflections output	5248	5656	5271	5285	5282	5271	5478	5529
Wavelength normalization								
Overall R factor (intensity), %	8.9	14.9	8.9	9.2	9.0	10.4	8.1	8.9
Multiple-measured reflections	1647	1121	1435	1378	1374	1210	1305	1157
Final data set								
Total structure factors	3148	3229	3233	3099	3120	2974	3262	3423
Completeness of data, %	26	26	27	25	26	24	27	29
R factor vs. monochromatic data, %	9.3	16.2	10.6	9.7	9.6	10.1	9.9	8.9
Structural statistics†								
Total atoms	1753	1736	1735	1736	1736	1736	1736	1751
Bond distance (rms)	0.022	0.024	0.020	0.022	0.022	0.018	0.020	0.024
Angle distance (rms)	0.056	0.058	0.051	0.053	0.053	0.045	0.053	0.056
Planar group (rms)	0.028	0.028	0.027	0.028	0.027	0.023	0.027	0.028
Refinement R factor,‡ %	17.2	22.9	18.9	18.2	18.7	19.1	18.8	18.1

*All data sets are to 2.5-Å resolution.
†All rms values are the average deviation of the parameter listed relative to the ideal restrained deviations defined as follows: bond distance, 0.020 Å; angle distance 0.030°; planar groups, 0.025 Å.
‡$R = \Sigma (F_{obs} - F_{calc})/\Sigma (F_{obs})$.

the increase in A_{402} was monitored. Assays were for 150 sec; the final slope was used to determine enzymatic activity, to ensure that the system was at a steady state (23).

RESULTS

Crystallographic Studies. The mechanisms of the light-induced cinnamate deacylation and the binding of pyrone are shown in Fig. 3. Examination of the protein difference maps calculated directly after the initial refinement shows the clear presence of the cinnamoyl group before photolysis and the expected final acyl pyrone derivative at t = +24 hr. Free enzyme is observed as soon as 1 min after photolysis, persisting >20 min after irradiation. These structures compare favorably in quality and in detail with those determined previously by monochromatic crystallography (17–19). The t = 0 difference map shows electron density in the active-site aromatic binding pocket that has the approximate dimensions and appearance of a weakly bound, 10-membered bicyclic coumarin ring. This map contains no definitive features of the diethylamino substituent and the ring orientation is therefore difficult to model unambiguously in the pocket.

Structure of the cinnamate bound to chymotrypsin (t = −5 *min*). This inhibitor shows a bound geometry identical with that observed previously (18, 19). The compound is covalently bound to the active-site serine with a bond distance of 1.5 Å, a bond angle of 125° through the carbonyl carbon, and a trans geometry through the α-carbon double bond. The inhibitor has a planar geometry. The hydroxyphenyl ring is found in the specificity pocket flanked by the backbone of residues 190–195 and 214–217. The para amino nitrogen is visible and participates in a polar interaction with the backbone oxygen of residue 217 as previously observed. The acyl oxygen points away from the oxyanion hole due to the lack of rotational freedom about the sp^2 hybridized carbon. Difference maps of the inhibitor complex are shown in Figs. 4 and 5.

Structure of the photolysis product (t = *0 min*). The diffraction pattern collected concurrently with photolysis shows streaking of the individual spots on the film. This streaking disappears in subsequent exposures, consistent with a temporary internal disordering of the crystal lattice during the flash, as observed in earlier monochromatic studies of photolysis (19). This disorder causes a significant deterioration in the final statistics for the data set and the refinement. Examination of the resulting $F_o - F_c$ map shows protein density that is still clean and free of noise but disjointed throughout the map relative to other time points. Examination of the active site shows that the nucleophilic serine γ-oxygen is free of covalently bound inhibitor and has moved by 0.8 Å relative to the cinnamate-bound complex, with a 35° rotation about the C^α–C^β bond. The specificity pocket shows the presence of density that is of the approximate size and shape of a bicyclic coumarin ring. This density is found in a planar orientation similar to that of the phenyl ring of the cinnamate but appears to be rotated within the plane of the ring relative to the cinnamate density (Figs. 4 and 5). The density is of poor quality, with an absence of density for the diethylamino group, making the structure difficult to model unambiguously.

Structure of free enzyme (t = *+1 min*). The electron density map is fit well by a model identical to that determined previously from monochromatic data collection after photolysis (19). The serine side chain is unchanged from the t = 0 time point, with clear density that terminates at the γ-oxygen. The specificity pocket shows density at a 2σ contour level that appears to reflect the presence of bound solvent, salt, or nonphotolyzed inhibitor. Lowering the contour level close to the noise level of the map, however, shows the density to correspond to a low occupancy of noncovalently bound peptide that is found in the active site of crystalline chymotrypsin (14, 20) and that is not displaced by the cinnamate ester during the crystal soak. This density is present at the next three time points (5, 10, and 20 min).

Structure of pyrone-bound complex (t = *+3 to +24 hr*). By 3 hr after flash, density is apparent that is consistent with pyrone bound in a conformation similar to that reported by Ringe *et al.* (17). At 24 hr, difference maps clearly reveal fully bound pyrone in the active site (Figs. 4 and 5). This density is distinct from that observed for bound cinnamate, due to the nonplanar sp^3 carbon extending from the phenyl ring, which is bound in the specificity pocket. The inhibitor is covalently bound to the serine with a bond length of 1.8 Å and exists as an extended molecule that is formed after ring opening, hydrolysis, and formation of a polar interaction with His-57 as described previously. Initial modeling of the density was performed by a rigid-body superposition of model coordinates for bound pyrone from the previous structure. The distance from the terminal carboxyl oxygens of the inhibitor to the ε2 nitrogen of His-57 is ≈3.0 Å.

Solution Studies. The activity of the inhibited enzyme prior to irradiation is ≈3% of the photoactivated chymotrypsin activity. Although it is difficult to precisely quantitate the recovery of activity after photolysis relative to native enzyme (because the acylated enzyme is purified over a gel filtration column), the enzyme regains >90% of its specific activity after irradiation. With pyrone present, the enzymatic activity then decreases as a function of time with an approximate first-order rate constant for inactivation of 1.06×10^{-2} min^{-1} and a half-life of 65 min. In the absence of pyrone, photolysis produces a rapid recovery of activity with no subsequent decrease (Fig. 6).

DISCUSSION

Data Collection Strategy. Covalently bound cinnamate was photolyzed from the active site to ensure that diffusion would not serve as the rate-limiting step of turnover. Such methods do not guarantee synchronized catalysis but rather ensure

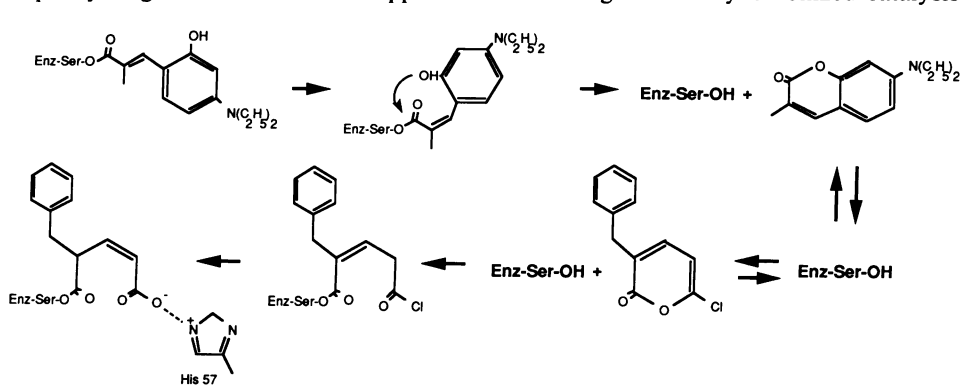

FIG. 3. Reaction sequence for the light-induced binding of pyrone.

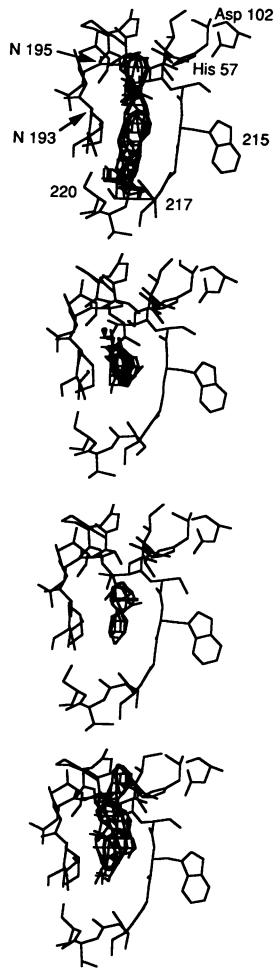

FIG. 4. Difference Fourier maps of the P1 binding site of chymotrypsin at four time points during the reaction. The four time points shown are (top to bottom) $t = -5$ min (prior to photolysis), $t = 0$ min (concurrent with photolysis), $t = +1$ min, and $t = +24$ hr. All maps are $F_o - F_c$ syntheses calculated using the coordinates from the initial round of least-squares refinement against the appropriate data set. No inhibitor or solvent coordinates were included in the refinements or the phase calculations.

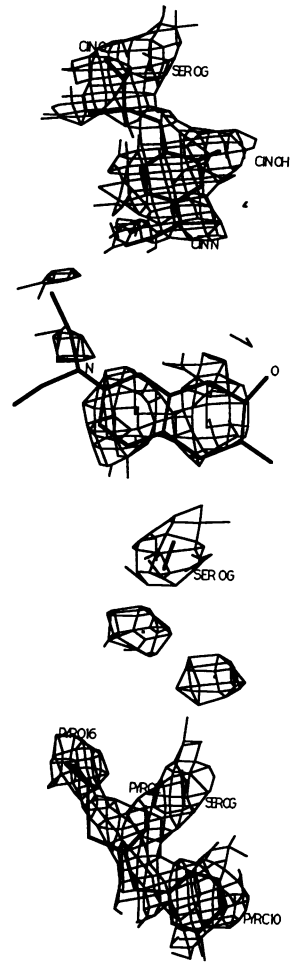

FIG. 5. Difference Fourier maps of the P1 binding site of chymotrypsin at the same four time points as in Fig. 4. All four maps are viewed perpendicular to the plane of the cinnamate ring in the first map. SER OG, serine γ-oxygen; CIN, cinnamate; PYR, pyrone.

that the accumulation and decay of an intermediate that directly precedes a rate-limiting kinetic barrier will occur in a concerted manner, i.e., with the participation of a high percentage of the population. The exact yield of an intermediate during turnover is a function of the efficiency of the photoreactive trigger and of the magnitude of the kinetic barriers preceding the formation of the intermediate for each enzyme molecule in the crystal lattice.

Data were collected using one exposure per time point. This strategy lowers the percentage of the reflections collected in any given data set but also lowers the time interval over which conformational averaging occurs. Laue structural studies with ≤25% of a complete data set have been shown to yield interpretable maps. For example, Laue data sets with only 16% of the possible data from 6 to 3 Å were used to calculate Fourier difference maps of xylose isomerase (13) that clearly showed metal binding sites. Similarly, Laue data sets with 25% of the possible data to 2.4-Å resolution were used to calculate difference maps that showed the oligosaccharide-binding site in phosphorylase *b*, with a map quality that "compared favorably with the corresponding difference Fourier synthesis calculated with the equivalent measurements from the monochromatic data set" (1).

Quality of Polychromatic X-Ray Data. One of the strengths of polychromatic x-ray diffraction data collected at a synchrotron is the quality of the data. This is due to a high signal/noise ratio produced by a very intense x-ray beam that is well collimated and shielded, leading to relatively low background and correspondingly more reliable measurements of intensities for each reflection. In addition, radiation damage is uniformly represented over the entire diffraction pattern during the short period of a single x-ray exposure.

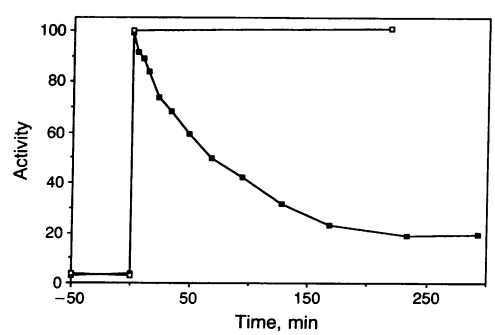

FIG. 6. Regeneration and loss of chymotrypsin activity in solution, produced by photolysis of bound cinnamate in the presence (■) or absence (□) of pyrone. Photolysis was accomplished by 40 sec of irradiation with the 366-nm emission line from a 500-W Hg lamp. The activity measured immediately after photolysis was assigned as 100%.

The data set in the present study for which the above generalizations are not as true is $t = 0$, collected concurrently with photolysis. As described earlier, photolysis causes a transient streaking in the observed reflections throughout the film. This phenomenon was also observed under different conditions in Laue photographs of phosphorylase *b* during diffusion of substrate into the enzyme active site (1). This phenomena may be an effect that often occurs during a dynamic process in the crystal.

Quality of the Protein Difference Maps. The maps calculated from the various data sets used in this study are encouraging in their quality. The lack of low-resolution terms in the Fourier transform has not previously caused difficulties in analyses of difference maps; in fact, it is common practice to ignore these terms in refinements and subsequent difference Fouriers. These studies also profit from the availability of previously solved high-resolution structures of the beginning and end points of the reaction (17, 18).

Correlation with Results from Solution. The maps calculated from $t = +1$ min to $t = +24$ hr show slow binding of pyrone after photolysis with no accumulation of rate-limited intermediates prior to the formation of the final bound conformation. In solution, steady state is achieved after photolysis in the presence of 5 mM pyrone in 4–5 hr; this appears to correlate with the presence of fully bound pyrone in the crystal at $t = +24$ hr, a 4- to 5-fold difference in the reactivity of the enzyme in the two environments. This rate reduction is consistent with that usually observed for protein crystals as opposed to solution, due to the restricted motion of protein in the lattice (24).

The Laue method should allow for the study of short-lived, rate-limited intermediates that accumulate in the crystal and possess a lifetime comparable to the period of data collection. It is apparent that several areas must be addressed on an individual basis for each system under investigation for such experiments to be performed routinely.

(i) Exposure times. The time needed for data collection must be minimized so that the structure of the intermediate of interest reflects a statistical majority of the chemical states contributing to the reflections collected. Data sets containing roughly 50% of the unique data may be collected from a well-ordered crystal of high symmetry. Exposure times as low as 5 msec are now routinely used for collection of high-resolution Laue data sets from synchrotron x-ray sources of sufficient intensity. Various groups are attempting to reduce the amount of time necessary to collect an interpretable Laue photograph. A 120-psec diffraction pattern from a lysozyme crystal has been recorded using the flux from a single electron bunch; 50–200 spots were observed (25).

(ii) Kinetic characterization of the system. Our failure to observe the structure of a pyrone-bound intermediate prior to the formation of the final complex is due to some combination of two effects: (*a*) the rate-limiting step of binding appears to be the initial acylation and ring-opening step and (*b*) the time points at which data were collected were not optimal for observing intermediates (if any) that may have accumulated in the active site during inhibition by pyrone. The obstacle of characterizing the kinetics of a reaction under the conditions being studied crystallographically may become the largest hurdle in determining the structure of transient chemical intermediates. A different kinetic obstacle may be the study of enzymatic intermediate complexes for systems that show no single, unique rate-determining step. This situation is observed quite commonly in enzyme-catalyzed reactions.

(iii) Characterization of the chemical mechanism. The goal of crystallographers involved in the study of enzymatic function is the complete characterization of the *structural* mechanism of catalysis, meaning the direct observation of all enzyme–ligand interactions during catalysis. To model an intermediate state, however, the investigator must have an accurate model of the *chemical* mechanism followed during turnover, in order to assign the correct chemical species to the active site at any time point.

We thank the staff at the Deutsche Elektronen Synchrotron for their superb technical assistance (as well as their hospitality), especially Dr. Keith Wilson; Drs. Greg Farber, P. Lynne Howell, and Steven Almo; Dr. Ilme Schlichting and Dr. Gert Rapp for assistance with the photolysis of the crystal; and the laboratory of Dr. Robert Abeles for kindly providing the pyrone inhibitor for these studies. B.L.S. was supported as a Whitaker College Health Sciences Fellow during the work described; the Petsko Laboratory was generously supported by Payload Systems, Inc., of Cambridge, MA.

1. Hajdu, J., Acharya, K. R., Stuart, D. I., Barford, D. & Johnson, L. N. (1988) *Trends Biochem. Sci.* **13**, 104–109.
2. Moffatt, K. (1989) *Annu. Rev. Biophys. Chem.* **18**, 309–332.
3. Moffatt, K., Szebenyi, D. M. E. & Bilderback, D. H. (1984) *Science* **223**, 1423–1425.
4. Helliwell, J. R. (1984) *Rep. Prog. Phys.* **47**, 1403.
5. Machin, P. A. (1985) *Inf. Q. Protein Crystal. Daresbury Lab.* **15**, 1–10.
6. Machin, P. A. (1987) in *Computational Aspects of Protein Crystal Data Analysis*, eds., Helliwell, J. R., Machin, P. A. & Papiz, M. Z. (Daresbury Lab., U.K.), pp. 75–83.
7. Campbell, J. W., Habash, J., Helliwell, J. R. & Moffat, K. (1986) *Inf. Q. Protein Crystal. Daresbury Lab.* **18**, 23.
8. Campbell, J. W., Clifton, I. J., Elder, M., Machin, P. A., Zurek, S., Helliwell, J. R., Habash, J., Hajdu, J. & Harding, M. M. (1987) *Springer Ser. Biophys.* **2**, 52–60.
9. Helliwell, J. R., Habash, J., Cruickshank, D. W. J., Harding, M. M., Greenhough, T. J., Campbell, J. W., Clifton, I. J., Elder, M., Machin, P. A., Papiz, M. Z. & Zurek, S. (1989) *J. Appl. Crystallogr.* **22**, 483–497.
10. Hajdu, J., Acharya, K. R., Stuart, D. I., McLaughlin, P. J., Barford, D., Oikonomakos, N. G., Klein, H. & Johnson, L. N. (1987) *EMBO J.* **6**, 539–546.
11. Hajdu, J., Machin, P. A., Campbell, J. W., Greenhough, T. J., Clifton, I. J., Zurek, S., Gover, S., Johnson, L. N. & Elder, M. (1987) *Nature (London)* **329**, 115–116.
12. Hajdu, J. & Johnson, L. N. (1990) *Biochemistry* **29**, 1669–1678.
13. Farber, G. K., Machin, P., Almo, S. C., Petsko, G. A. & Hajdu, J. (1988) *Proc. Natl. Acad. Sci. USA* **85**, 112–115.
14. Almo, S. C., Howell, P. L., Petsko, G. A. & Hajdu, J. (1991) *Proc. Natl. Acad. Sci. USA*, in press.
15. Schlichting, I., Almo, S. C., Rapp, G., Wilson, K., Petratos, K., Lentfer, A., Wittinghofer, A., Kabsch, W., Pai, E., Petsko, G. & Goody, R. (1990) *Nature (London)* **345**, 309–315.
16. Campbell, J. W., Clifton, I. J., Greenough, T. J., Hajdu, J., Harrison, S. C., Liddington, R. C. & Shrive, A. K. (1990) *J. Mol. Biol.* **214**, 627–632.
17. Ringe, D., Mottonen, J. M., Gelb, M. H. & Abeles, R. H. (1986) *Biochemistry* **25**, 5633–5638.
18. Stoddard, B. L., Bruhnke, J., Porter, N., Ringe, D. & Petsko, G. (1990) *Biochemistry* **29**, 4871–4879.
19. Stoddard, B. L., Koenigs, P., Porter, N., Ringe, D. & Petsko, G. (1990) *Biochemistry* **29**, 8042–8051.
20. Dixon, M. M. & Matthews, B. W. (1989) *Biochemistry* **28**, 7033–7038.
21. Rapp, G. & Guth, K. (1988) *Pflügers Arch.* **411**, 200–203.
22. Jones, T. A. (1978) *J. Appl. Crystallogr.* **11**, 268–272.
23. Westkaemper, R. B. & Abeles, R. H. (1983) *Biochemistry* **22**, 3256–3264.
24. Makinen, M. & Fink, A. (1977) *Annu. Rev. Biophys. Bioeng.* **6**, 301–342.
25. Szebenyi, D. M. E., Bilderback, D., LeGrand, A., Moffatt, K., Schildkamp, W. & Teng, T. Y. (1988) *Trans. Am. Crystallogr. Assoc.* **24**, 167–172.